Updated 08/15/2021

MCS data postProcessing manual

CNS Biophysics Lab.

Eun-Kee (E.K.) Jeong, Ph.D.

Utah Center for Advanced Imaging Research
Dept. of Radiology and Imaging Sciences
University of Utah
Salt Lake City, UT 84108

INTRODUCTION

Typical cell is surrounded by a single lipid bilayer, which is composed of cholesterol, phospholipid, and glycolipid by 4:3:3 ratio. Through this single lipid bilayer, it is difficult for any charged or large molecules, such as Na^+, K^+, protein, to penetrate without help from ATP (active transport). It is almost freely exchangeable for most small neutral molecules, including O_2. CO_2, and H_2O. The permeability of water molecule through cell has been reported as 30 ~ 700 μm/s.

Axon in central nerve system (CNS) is protected by many tens of lipid bilayers, myelin sheath, except at the node of $Ránvier$ (~1 % portion). It is almost impermeable for water molecules across this myelin sheath. The water permeability P, however, through this myelin is not zero, but rather a few, say P < 10 μm/sec due to the node of $Ránvier$. The white-matter which consists of bundle of axons running parallel to each other, has orientation preference, along which the water molecules can almost freely move. One can assign three spaces in white-matter; intra-axonal (IA) and extra-axonal (EA) spaces, and myelin space (MS).

IA water diffusion is highly restricted by the myelin sheath, whose main role is to confine the charged ion particles within the IA space, except at the nodes of $Ránvier$. Although there are hindered water diffusion due to the membranes at specific organelles, such as nucleus, oligodendrocytes, neurons, and immune cells, water molecules can still migrate in and out of those boundaries, unlike those in the myelinated axon with tens lipid-bilayers. Therefore, for the "**radial DWI**", heterogeneous physical environment inside the CSC white-matter may be compartmented into, (1) "*restricted*" IA space where water cannot move more than diameter of the axon (~1.2 μm [1]), and (2) all other "*mobile*" space which water can move over the hindered boundaries including the membranes. At sufficiently high DW and with a long echotime (> 5*T_2), we observed DWI signal from "*mobile*" water protons in extra-axonal (EA) and myelin space almost suppressed down to background noise level, which leaves only the signal contributed from IA water. We have observed this behavior on radial UHB-DWI from <u>*all*</u> in- and ex-vivo CSC [2–7]. Detail about current software is described in our previous reports [2,3,7]

Monte-Carlo Simulation (MCS): We developed an MCS software using Python and MPI (Message Passage Interface) C++, utilizing the parallel computing on linux clusters. The software was developed using Python 3.x language, particularly SymPy [8] for symbolic calculation, NumPy [9] and SciPy [10] for array processing, and matplotlib [11] for plotting and displaying data. The software uses either a microscopic image or an internally generated geometry with user-defined size distribution, distributes water molecules, simulates random hoppings and records positions of all molecules and timepoints for a user-defined simulation parameters, as in GUI window above, including permeability. Using this position data, DW signal is calculated for a specific DWI scheme as described in our recent reports [2,3]. *The software can adapt any user-defined geometry, such as for demyelination, inflammation, and axonal beading.*

MCS for normal CSC: Plots in Fig.1 show simulated radial DWI signal with $\mathbf{G}_D$ applied in radial (⊥) to the fiber direction. Fig. 1(b) indicates that calculated diffusivity for the total signal decreases with increasing b-value due to increased fraction of IA water signal, and <u>*is not objective but dependent on b-value*</u>.

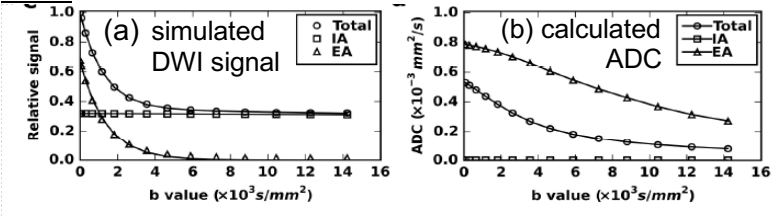

Fig. 1. *Simulated radial UHb-DWI for a MCS result for a pig optical microscopy in Fig. 5: (a) signal-b and (b) diffusivity curves for the total* (o), *intra-* (□) *and extra-axonal* (*Δ*) *signals, using δ = 30 ms and Δ = 0.45 s. Note that ADC value decreases with increased b-value.*

Fig. 2 illustrates measured rDWI and aDWI signals with respect to b-value in white-matter (Fig. 2a) and gray-matter (Fig. 2b) of a fresh pig CSC. The rDWI signal of the white-matter indicates that there are

clearly two distinct signals, i.e., fast- and slow-decaying signals, while that of aDWI signal fits to a single-exponential function. These signal-b behaviors can be obtained using a set of numerical monte-Carlo Simulation of the water diffusion within white-matter.

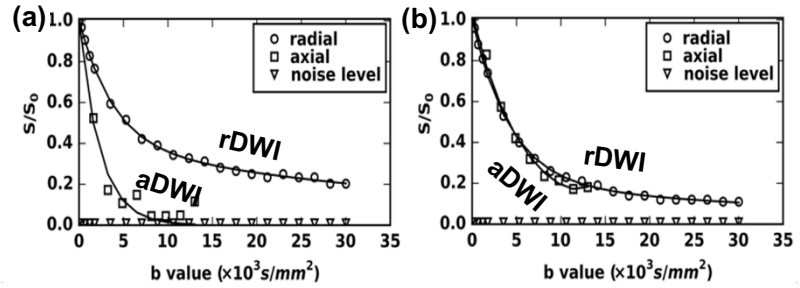

Fig. 2. *UHb-DWI signal-b curve on fresh ex-vivo pig CSC; (a) WM and (b) GM with axial (□) and radial (O) signal. The axial DWI signal in WM in (a) quickly decays to low plateau level indicating little barrier, but that in GM in (b) shows higher restriction than axial WM signal.*

Post-Processing of MCS data: We have obtained sets of MCS data from a parallelized Linux-cluster with 250 ms total diffusion time, 1.0 μs hopping time (Δt_{calc}), 100 μs saving time for 3199 synthetic axons with γ-variate distribution, which were randomly distributed on an 80x0 μm^2 imaging pixel, which is divided to 2500x2500 grids with grid size of 32x32 nm^2. The mean displacement is 134 nm for D = 3.0x10^{-3} mm^2/s and hopping time 1.0 μs, which were used to generate the sample MCS data. Axons run parallel to each other along z-axis and 3D diffusion was performed with the instantaneous hopping with gaussian probability with the mean displacement of $\sqrt{6D\Delta t_{calc}}$. Included MCS data contain information about the axons, initial and all transient position vectors of 10,000 water molecules for 250 ms and whether a molecule resides within intra-axonal (IA), myelin (ML), or extra-axonal (EA) space at any saved time point. The post-processing software reads all these data and generates a synthetic signal-b curve for a pair of diffusion gradient in either spin-echo or stimulated-echo DWI.

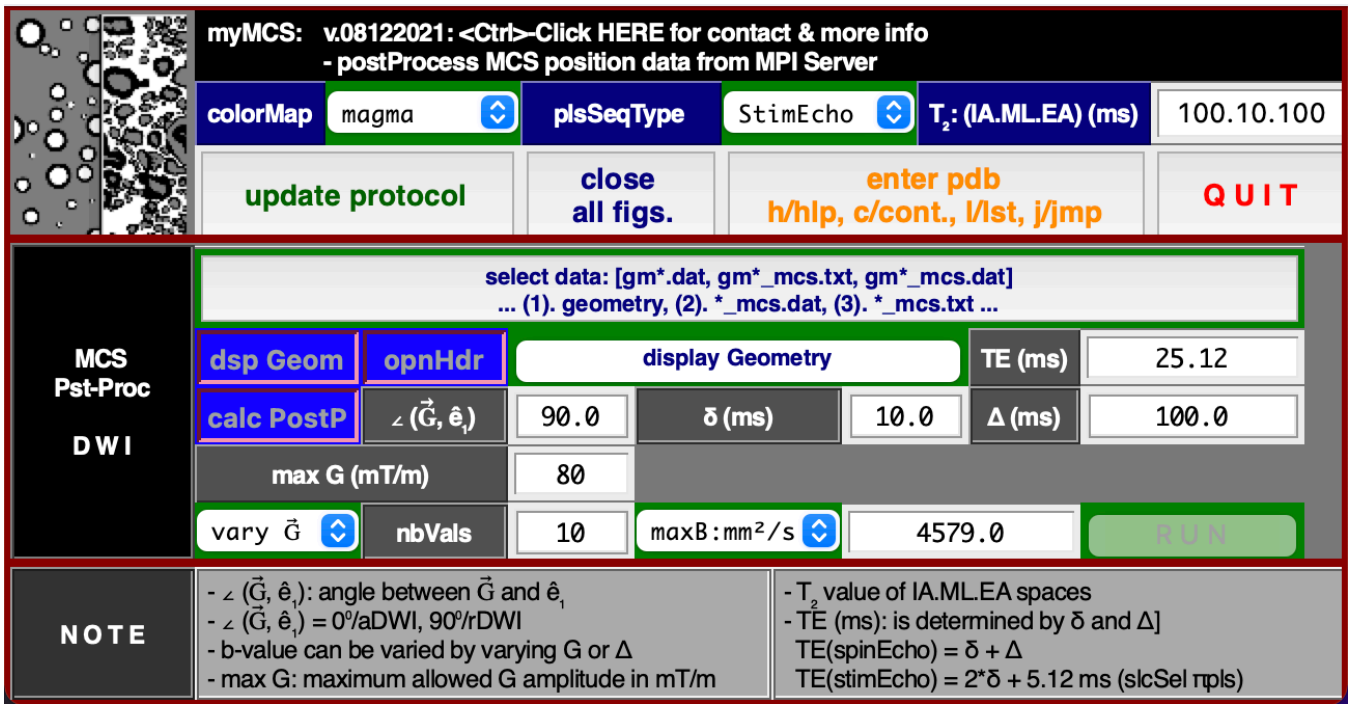

Fig. 3. *GUI-Frontend of PostProcessing software. The software is launched by python myMCS.py.*

MCS Post-Processing: The position data is read and processed for a specific diffusion waveform. We use a bipolar diffusion waveform with a pair of G_d with duration δ, separated by Δ.

- **Select MCS data**: Three files (preprocessed *geometry.dat*, and two MCS output files, *geometry*_mcs.txt, geometry*_mcs.dat*) must be selected for post-processing.

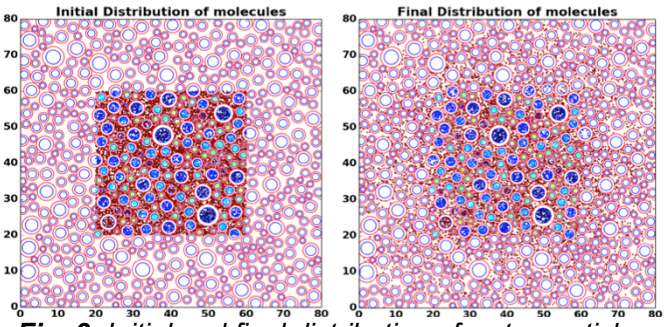

***Fig. 3**. Initial and final distribution of water particles.*

- 

: **calc PostP**: Angle (°) between the diffusion gradient $\vec{G}_D$ and axon's principal axis ($\hat{z}$) for single direction DWI. Set 0° to evaluate axial DWI signal-b curve.

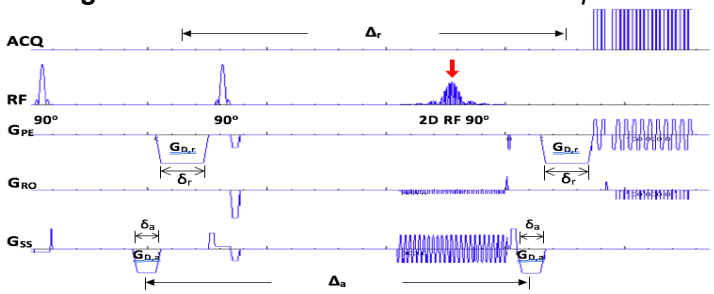

***Fig. 4**. 2D ss-DWSTEPI, with short δ and large Δ, but with 50 % loss of diffPrep magnetization during tipUp 90°.*

- 

: Duration and separation of diffusion gradient $\vec{G}_D$ in *ms*. The practical values are $\delta > 10\ ms$ and $\Delta = 100 \sim 400\ ms$ for stimulated-echo DWI at a wholebody clinical MRI system, of which gradient performance is in general limited by nerve stimulate by $dB/dt < 100\ mT/m/s$. The maximum Δ can't be larger than $T_{diff} - \delta$, i.e., $\Delta < T_{diff} - \delta$. The signal at the timepoint t_m is calculated by vector summation of all spins as in,

$$M_+(\vec{G}_D; t_n) = \sum_{m=0}^{N_{mols}} e^{-t_n/T_{2,m}}\, e^{-i\theta_{m,n}(t_n)}, \quad \theta_{m,n}(t) = \gamma \int_0^{t_n} \vec{G}_D(t) \cdot \vec{r}_m(t) dt \qquad \dots (D1)$$

Here, $\theta_{m,n}(t)$ indicates the phase-accumulation for m^{th} spin at time t_n. All spins are assumed to be polarized, after the Boltzmann distribution. The eq. (D1) tells us that the m^{th} spin, i.e., the m^{th} water molecule, contributes to the total signal as a 2D vector with its phase $\theta_{m,n}(t)$.

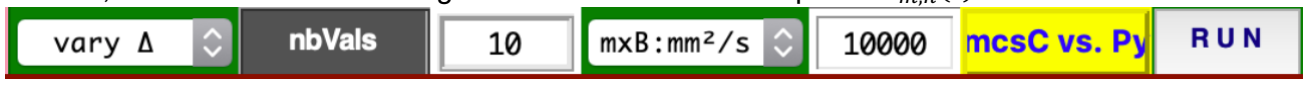

- **Ultra-high-B DWI (UHb-DWI)**: The position data is used to simulate the signal-b curve for a specific $\vec{G}_D$ direction with respect to the axonal pathway ($\hat{z}$).
  - **Vary $\vec{G}_D$:** This technique is not used for UHb-DWI at clinical MRI system with low gradient amplitude, because of long TE. But it may be usable at modern MRI system which is equipped with increased gradient performance, such as Siemen's Prisma with 80 mT/m gradient strength.
  - **Vary Δ:** In actual measurement, there will be T_1 decay during the mixing time TM in DWSTEI sequence, which needs to be corrected using a data set with $G_D = 0$.
  - **Constant b with variable Δ:** Ideal for measuring permeability effect. In practice, the time-efficiency will be low, because of requiring up to a long Δ_{max}.

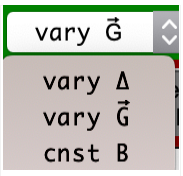

  - 

: Maximum b-value in s/mm². In clinical imaging, we typically reach up to b_{max} = ~ 10,000 s/mm².
  - 

: ΔG for "**Vary $\vec{G}_D$**" to vary b-value.
  - 

: $\Delta_{increment}$ for "**Vary Δ**" to vary b-value.

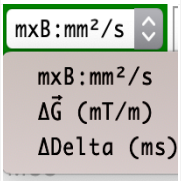

. **Calculate decay constant D_H**: The signal-b curve is fit to a double-exponential function $S(b) = S_F e^{-bD_F} + S_H e^{-bD_H}$, with IA fraction (IAF) = S_H/S_o. The experimental data is fit pixel-by-pixel, after subtracting the background noise value. If the fraction of the high-b signal is less than that for 5*stdDev of the noise, i.e, $S_H/S_o < 5*stdDev_{noise}/S_o$, which is the case with significant water exchange between IA and EA spaces, signal-b is fit to a single-exponential function $S(b) = S_o e^{-bD_H}$, in which case IAF can't be defined.

MCS data

MCS data for MS1 and MS2 patients are included. Each set consists of three sets of data: (1) healthy, (2) lesion, and (3) narmal appearing white-matter (NAWM). These MCS data were generated for specific set of pathologic parameters, such as fraction of demyelination among 3199 axons, water permeabilities of healthy and demyelinated axons at the axonal membrane. Each folder containes three files, which all three files must be selected during file-selection.

(1) intial input data to MCS process (filename: C3199_L80D12A4B6_W10kR66_Dm55Da0_2k.dat)

(2) position data for all molecules at all time points (filename: C3199_L80D12A4B6_W10kR66_Dm55Da0_2k_TT250.0C1.00S100_P85.100PB1_mcs.dat)

(3) MCS simulation parameters (filename: C3199_L80D12A4B6_W10kR66_Dm55Da0_2k_TT250.0C1.00S100_P85.100PB1_mcs.txt)

REFERENCES

(1) Kim, T. H.; Zollinger, L.; Shi, X. F.; Rose, J.; Patel, A. A.; Jeong, E. K. Quantification of Diffusivities of the Human Cervical Spinal Cord Using a 2D Single-Shot Interleaved Multisection Inner Volume Diffusion-Weighted Echo-Planar Imaging Technique. *AJNR Am J Neuroradiol* **2010**, *31* (4), 682–687.

(2) Sapkota, N.; Yoon, S.; Thapa, B.; Lee, Y.; Bisson, E.; Bowman, B.; Miller, S.; Shah, L.; Rose, J.; Jeong, E. Characterization of Spinal Cord White Matter by Suppressing Signal from Hindered Space. A Monte Carlo Simulation and an Ex Vivo Ultrahigh-b Diffusion-Weighted Imaging Study. *J. Magn. Reson.* **2016**, *272*, 53–59.

(3) Sapkota, N.; Rose, J.; Miller, S.; Bowman, A.; Shah, L.; Bisson, E.; Yoon, S.; Jeong, E. K. Estimation of Intra-Axonal Fraction in Spinal Cord White Matter by Using Monte Carlo Simulation of Water Diffusion and High b-Value Diffusion Sensitized MRI. In *the 23rd annual ISMRM*; Toronto, Canada, 2015; Vol. 23, p 3044.

(4) Lee, S. Y. J.; Thapa, B.; Sapkota, N.; Kim, E. J.; Shah, L. M.; Rose, J. W.; Jeong, E. K. Ultrahigh-b Diffusion Imaging of Cervical Spinal Cord in Multiple Sclerosis. In *2017 Annual Meeting of ISMRM*; Honolulu, HI, USA, 2017; p 2561.

(5) Thapa, B.; Sapkota, N.; Lee, Y.; Shah, L.; Rose, J.; Jeong, E. Signal Behavior of Ultra-High-b Radial Diffusion Weighted Imaging (UHb-RDWI) Signal in Different Tract of the Cervical Spinal Cord. In *2017 Annual meeting of ISMRM*; Honolulu, HI, USA, 2017; p 1876.

(6) Jeong, K. E.; Shah, L. M.; Lee, S. Y.; Thapa, B.; Sapkota, N.; Bisson, E. F.; Carlson, N. G.; Jeong, E. K.; Rose, J. W. High-b Diffusivity of MS Lesion in Cervical Spinal Cord Using Ultrahigh-b DWI (UHb-DWI). *NeuroImage:Clinical* **2021**, *30*, 102619.

(7) Jeong, K. E.; Lee, S. Y. J.; Yeom, S. K.; Carlson, N. G.; Shah, L. M.; Rose, J. W.; Jeong, E. K. Ultrahigh-b DWI (UHb-DWI) for Quantitative Evaluation of Myelination in Shiverer Mouse Spinal Cord. *Magn Reson Med* **2021**, *in-print*, PMID: 34418157 DOI: 10.1002/mrm.28978. https://doi.org/10.1002/mrm.28978.

(8) Aaron, M.; Smith, C. P.; Paprocki, M.; Čertík, O.; Kirpichev, S. B.; Rocklin, M.; Kumar, Am.; Ivanov, S.; Moore, J. K.; Singh, S.; Rathnayake, T.; Vig, S.; Granger, B. E.; Muller, R. P.; Bonazzi, F.; Gupta, H.; Vats, S.; Johansson, F.; Pedregosa, F.; Curry, M. J.; Terrel, A. R.; Roučka, Š.; Saboo, A.; Fernando, I.; Kulal, S.; Cimrman, R.; Scopatz, A. SymPy: Symbolic Computing in Python. *PeerJ Comput. Sci.* **2017**, *3*, e103.

(9) Van Der Walt, S.; Colbert, S. C.; Varoquaux, G. The NumPy Array: A Structure for Efficient Numerical Computation. *Comput. Sci. Eng.* **2011**, *13* (2), 22–30. https://doi.org/10.1109/MCSE.2011.37.

(10) Oliphant, T. E. SciPy: Open Source Scientific Tools for Python. *Comput. Sci. Eng.* **2007**, *9*, 10–20.

(11) Hunter, J. D. Matplotlib: A 2D Graphics Environment. *Comput. Sci. Eng.* **2007**, *9* (3), 99–104. https://doi.org/10.1109/MCSE.2007.55.